Transition from negative to positive photoconductivity in p-type $Pb_{1-x}Eu_xTe$ films

M. J. P. Pirralho,[1] M. L. Peres,[1,*] D. A. W. Soares,[1] P. C. O. Braga,[1] F. S. Pena,[1] C. I. Fornari,[2] P. H. O. Rappl,[2] and E. Abramof[2]

[1]*Instituto de Física e Química, Universidade Federal de Itajubá, Itajubá, MG CEP 37500-903, Brazil*

[2]*Laboratório Associado de Sensores e Materiais, Instituto Nacional de Pesquisas Espaciais, São José dos Campos, Paraíba 515, SP CEP 12201-970, Brazil*

(Received 8 September 2016; revised manuscript received 14 January 2017; published 8 February 2017)

We investigated the photoconductivity effect in p-type $Pb_{1-x}Eu_xTe$ films for $x = 0.01$, 0.02, 0.03, 0.05, and 0.06 at $T = 300$ K. The measurements revealed a clear transition from negative to positive photoconductivity as the Eu content x is increased at room temperature. This transition is related to the metal-insulator transition that occurs due to the disorder originated from the introduction of Eu atoms and it is an Anderson transition. Our investigation found that, from the potential application point of view, the sample $x = 0.06$ is more suitable, i.e., it presents an almost noise-free signal and the higher photoconductivity amplitude response. The photoconductive amplitude response for the sample with $x = 0.06$ was investigated further in the temperature range of 77–300 K and, surprisingly, multiple additional transitions were observed with amplitudes that reached around 200 times the original value before illumination. We show that this anomalous behavior is a consequence of the generation and recombination rates between the bands and the $4f$ level and a defect level located inside the band gap.

DOI: 10.1103/PhysRevB.95.075202

I. INTRODUCTION

The phenomenon of photoconductivity has been used as an important tool to investigate the presence of additional states within the band structure of semiconductors [1,2] and has provided basic knowledge that allowed the development of photodetector and sensor devices during the past decades [3–5]. Also, the persistent photoconductivity (PPC) effect where the value of the conductivity does not recover its original values after the illumination is removed is an important tool to determine the values of trap depths originated from defect states.

Recently, the effect of negative photoconductivity, i.e., the reduction of the electrical conductivity under illumination, has attracted some attention due to its potential application in the development on new photonic devices and nonvolatile memories with low power consumption [3]. Among the most recent investigated materials that exhibit the negative photoconductivity (NPC) effect are as follows: MoS_2 monolayers [6], In_2Se_3 films [7], silk protein hydrogels [8], films of functionalized metal nanoparticles [9], and antimony sulfoiodide nanowires [10], just to cite a few examples. Also, NPC is a phenomenon observed in degenerate systems and was observed in several semiconductors, such as InN [11], PbTe(Ga) [12], n-PbTe (Ga) [13], $Pb_{1-x}Ge_xTe$ alloys [14]. In addition, this phenomenon has been observed in a variety of semiconductor nanostructures, such as p-type carbon nanotubes, Bi-doped p-type ZnSe nanowires, n-type InN thin films, etc. [3]. For most of these materials, the NPC effect is a consequence of trap levels inside the band gap. For n-type PbTe:Ga films, the NPC effect was detected at low temperatures (∼4.2 K) and was described as a result of the generation-recombination processes in the system in the presence of impurity levels introduced by Ga [13]. For undoped PbTe samples, spectral photoresponse experiments showed that a defect level is present within the energy gap due to the intrinsic disorder generated during the sample growth [15]. Recently, it was found that $Pb_{1-x}Sn_xTe$ films also present the NPC effect due to trap centers that are close to the valence-band maximum when Sn content is around 0.40 [16]. For $Pb_{1-x}Eu_xTe$ alloys here we report about the positive or negative photoconductivity effect. It is well known that the introduction of Eu atoms alters drastically the electrical and optical properties of this heterostructure and one can expect that this could also play some role in photoconductivity experiments.

PbTe is a narrow gap semiconductor from the IV-VI family and is widely used in the fabrication of detectors and sensor devices operating in the range of visible to infrared radiation. PbTe samples are in general highly degenerate and present a metallic like behavior with high carrier mobility at low temperatures due to its large dielectric constant ($\varepsilon \sim 1350$ at 4.2 K) [17]. In addition, the physics is further enriched by the large value of the Landé g factor and the small effective mass; both of which display considerable anisotropy. Such properties make PbTe an interesting material for possible applications in spintronics [17]. As said before, the introduction of Eu^{2+} ions to form the $Pb_{1-x}Eu_xTe$ alloy drastically changes the optical and electrical properties of this compound [18]. The controlled inclusion of Eu content allows for tuning the fundamental absorption gap over a wide-energy range, i.e., from $E_g = 0.334$ eV for PbTe up to $E_g = 2.25$ eV for EuTe at $T = 300$ K [19]. In addition, the increasing in the Eu content leads to a metal-insulator transition that occurs around $x \sim 0.05$ for p-type samples and around $x \sim 0.1$ for n-type samples [18–20]. Another important consequence of the introduction of the Eu ions is the formation of the $4f$ level below the valence-band maximum for $x < 0.06$. For $x \sim 0.06$, the $4f$ level broadens with the valence-band maximum, and for $x \geqslant 0.06$ the $4f$ level is located in the band gap. Through optical measurements it was verified that in this situation the original transitions between the L_6^+ and the L_6^- points (valence and conduction bands, respectively) change to transitions between the $4f$ states and the L_6^- point. The influence of the $4f$ level on transport properties was investigated, and

*Corresponding author: marcelos@unifei.edu.br

 ©2017 American Physical Society

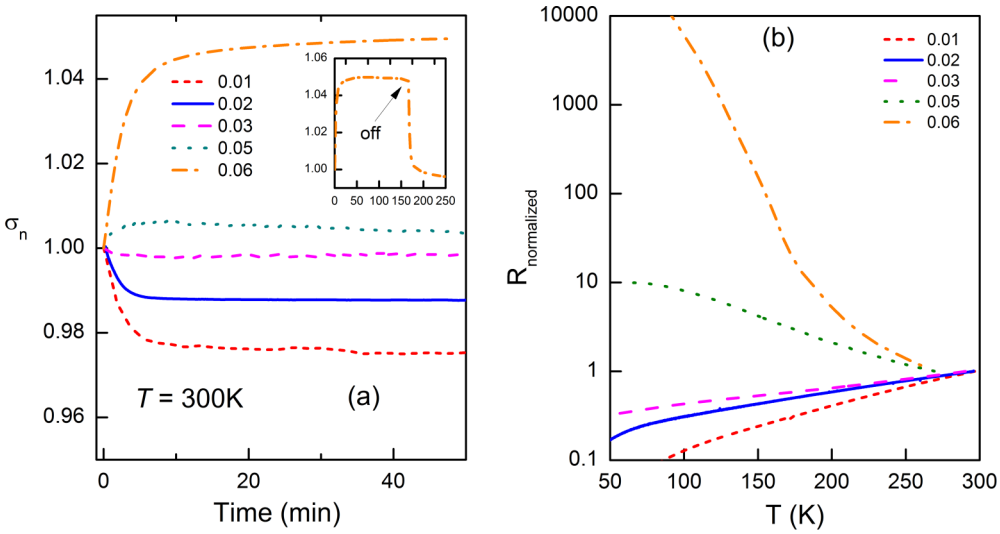

FIG. 1. (a) Normalized photoconductivity curves obtained for p-type $Pb_{1-x}Eu_xTe$ films for $x = 0.01, 0.02, 0.03, 0.05$, and 0.06 at $T = 300$ K under IR light excitation. This figure shows a clear transition from negative to positive photoconductivity as the Eu content x is increased. (b) Normalized electrical resistance as a function of temperature for $x = 0.01$, 0.02, 0.03, 0.05, and 0.06. As expected the metal-insulator transition can be observed around $x \sim 0.05$ (see the text for further explanation).

the strong influence of this level was verified in transport for insulating p-type $Pb_{1-x}Eu_xTe$ samples [20]. Regarding photoconductivity measurements, the influence of the $4f$ level was an open question, and we found that not only $Pb_{1-x}Eu_xTe$ samples give a high response to light, but also $Pb_{1-x}Eu_xTe$ samples present the anomalous negative photoconductivity effect.

The main goal of this paper is to perform a prospective study of NPC effect in p-type $Pb_{1-x}Eu_xTe$ films on both sides of the metal-insulator transition aiming for possible new applications in the development of photonic devices that operate from low temperatures up to room temperature. Although there is a large amount of studies about photoconductivity in semiconductors, in special narrow gap semiconductors, little information exists for p-type $Pb_{1-x}Eu_xTe$ films. In this paper, we present photoconductivity measurements for p-type $Pb_{1-x}Eu_xTe$ for x varying from 0.01 to 0.06, and we show that a transition from negative to positive photoconductivity occurs as Eu content x increases. A detailed analysis was performed in the sample with $x \sim 0.06$, which presented a very clear signal and the higher amplitude response to infrared radiation for low temperatures. In addition, anomalous profiles were observed in different temperature ranges below room temperature, revealing a strong persistent photoconductivity effect. The high amplitude response and the nearly noise-free signal reveal a potential application of insulator films for the development of optical devices that could operate at low temperatures.

II. SAMPLE STRUCTURE AND EXPERIMENT

In this paper we investigated high quality samples of p-type $Pb_{1-x}Eu_xTe$ with x varying from 0.01 up to 0.07. The samples were grown in a Riber 32P molecular-beam epitaxy system onto freshly cleaved (111) BaF_2 substrates. The films were grown at a substrate temperature of 208.5 °C during 2 h with a deposition rate of 3.9 Å/s, resulting in a 2.8-μm layer thickness. Three effusion cells with PbTe, Eu, and Te_2 were used to grow the samples. Pb (Te) vacancies in PbTe crystals act as acceptors (donors), therefore it is possible to control the concentration and the type of carriers through the chalcogen source flux variation. To provide a p-type sample an excess of Te_2 was maintained during the growth. The flux rates from the individual effusion cells were measured with an ion gauge, which is mounted on the sample manipulator and can be rotated on the substrate growth position. To obtain crystals with different Eu contents, the ratio between the PbTe and the Eu flux rates was varied. Hall measurements were performed in a nitrogen open circuit system, and a 15-T He-cooled superconducting magnet using an ac current of 1 μA at 10.7 Hz was used for measurements of transport parameters at low T (~4.2 K). An infrared LED with a wavelength of 940 nm and 12 mW/m^2 was used for the photoconductivity experiments.

III. RESULTS AND DISCUSSION

Figure 1(a) presents the photoconductivity measurements performed for p-type $Pb_{1-x}Eu_xTe$ films for $x = 0.01$, 0.02, 0.03, 0.05, and 0.06 at $T = 300$ K. This figure shows a clear transition from negative to positive photoconductivity as the Eu content x is increased. For $x = 0.06$, the photoconductivity amplitude reaches its maximum saturation value as compared to the other samples and presents the effect of persistent photoconductivity as observed in the inset, i.e., the signal takes several minutes to return to its original value after the light is switched off (indicated by the arrow). This transition is related to the metal-insulator transition that occurs due to the disorder originated from the introduction of Eu atoms [21]. Figure 1(b) presents the electrical resistance as a function of temperature for $x = 0.01$, 0.02, 0.03, 0.05, and 0.06. As expected the metal-insulator transition can be observed around $x \sim 0.05$. For concentrations higher than 0.05, the $4f$ level penetrates the energy gap and starts to participate of the transport mechanism [20]. The positive photoconductivity effect observed in Fig. 1(a) can be a result of the contribution of

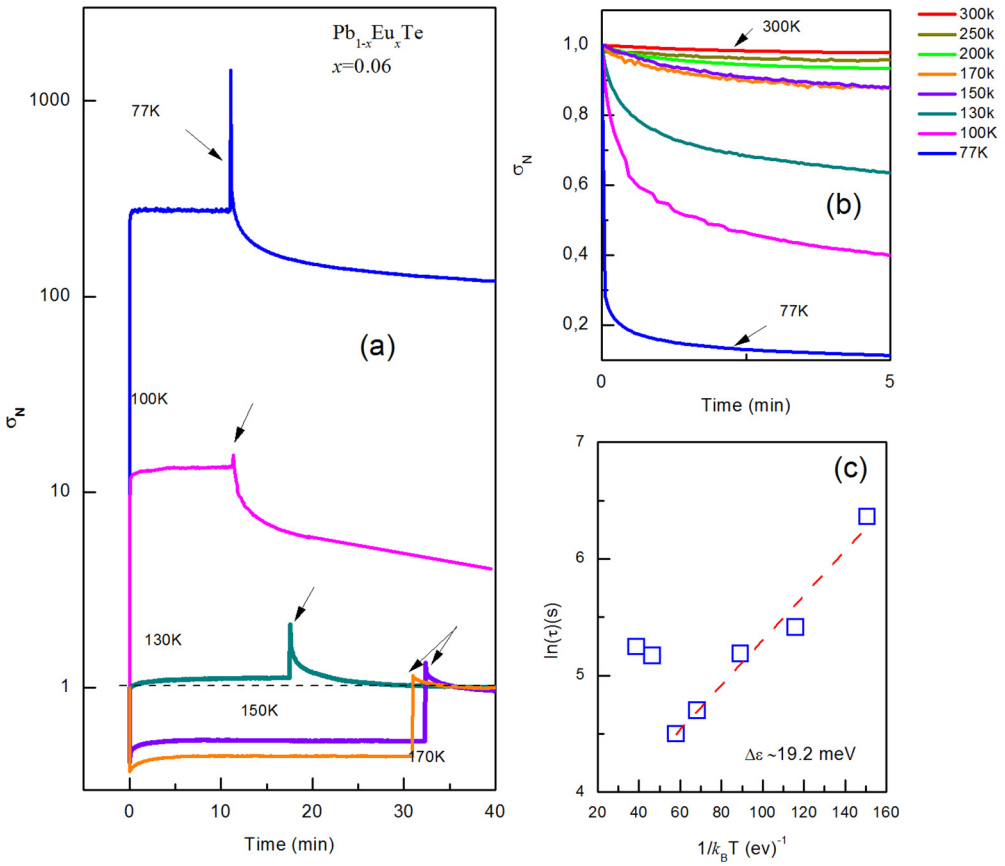

FIG. 2. (a) Normalized photoconductivity measurements performed for the film with $x \sim 0.06$ for temperatures of 77, 100, 130, 150, and 170 K. (b) Decay curves for all temperatures obtained from the measurements presented in (a). (c) Values of the logarithm of the recombination times as a function of temperature on a logarithmic scale. From a linear fitting, it is possible to obtain the depth trap energy responsible for the persistent effect, and the obtained value is 19.2 meV (±1 meV).

the $4f$ level in the generation and recombination mechanisms when the sample is illuminated. For the metallic samples, the negative photoconductivity can be a result of the contribution from defect levels located inside the energy gap [16]. From the potential application point of view, the sample with $x \sim 0.06$ is more suitable, i.e., it presents an almost noise-free signal and very high amplitude as mentioned before.

Figure 2(a) shows the photoconductivity measurements performed for the film with $x \sim 0.06$ for the temperatures of 77, 100, 130, 150, and 170 K. Surprisingly, the sample presented additional transitions and a remarkable response for IR light, reaching a value 200 times higher than the original value in dark conditions at $T \sim 77$ K. In fact, for the lower temperatures measured 77 and 100 K when the light is switched on, we observe an abrupt increase in photoconductivity. In general, the photoconductivity response depends on the competition of two mechanisms: the generation of carriers and the recombination of these same carriers. If both generation and recombination rates are the same, no photoresponse can be detected. The photoresponse, negative or positive, comes from the unbalance of these rates. Hence, if the generation/recombination ratio increases abruptly as temperatures decrease an abrupt increase in the photoresponse would be observed as in Fig. 2(a) at low temperatures. This will be discussed next. Also, the sample presents a strong persistent photoconductivity effect for $T < 130$ K, revealing the existence of trap levels that are more effective at low temperatures. Hence, the persistent photoconductivity effect is also temperature dependent since the carriers remain trapped for longer times as temperature reduces. The arrows in Fig. 2(a) indicate the positions when the light was off and where anomalous peaks are observed. This is because when the light is switched off, the photogeneration from the defect level and $4f$ level ceases and only recombination processes continue. In this situation, empty states that were being generated in these levels now remain occupied such that recombination from the conduction band to the defect and $4f$ levels is drastically reduced, i.e., there are less empty states to be filled. This transient regime presents an instantaneous increase in carrier in the conduction and valence bands, giving rise to the peaks observed in Fig. 2(a). As the electrons in the trap levels start to recombine back to the valence band, electrons from the conduction band start to recombine to the trap levels, and the peaks vanish. Similar peaks were observed in InN [5] and γ In_2Se_3 [7] films and are related to the influence of defect levels in the generation and recombination rates.

At low temperatures, the electrons remain longer trapped in the defect level since the detrapping by thermal energy is reduced. As a consequence, the conductivity does not recover its original value but remains at higher values instead.

One also observes that, for temperatures of 77, 100, and 130 K, the sample presents positive photoconductivity. As temperature is increased, a transition takes place, and the sample presents negative photoconductivity for temperatures of 150 and 170 K. Further increasing in the temperature leads to a second transition to a positive photoconductivity as that presented in Fig. 1(a) at 300 K and for $x \sim 0.06$.

Figure 2(b) presents the decay curves for all temperatures obtained from the measurements presented in Fig. 2(a). From these curves, we can obtain the recombination times using the expression $\sigma(t) = \sigma_0 \exp(-\frac{t}{\tau})$. Figure 2(c) exhibits the values of a natural logarithm of recombination times as a function of temperature. It is possible to obtain the trap depth energy responsible for the persistent effect by fitting the curve in Fig. 2(c) considering the expression $\tau = \tau_0 e^{\Delta\varepsilon/k_B T}$ [11]. The obtained value is 19.2 meV (±1 meV). This indicates that this energy is related to a trap level originated from defects and not from $4f$ levels since we know the position of the $4f$ level as will be see later in the text. Hence, the persistent effect comes from the defect level and not from the $4f$ level.

Hall-effect measurements also were performed in order to further investigate the IR light effect on the transport properties of the film. Figure 3(a) shows the Hall mobility under illumination (on) and dark conditions (off). Under dark conditions as temperature decreases, the mobility increases in the range of 300–250 K and diminishes between 250 and 200 K. Below this temperature, there is an increase in the mobility, suggesting that the main scattering mechanism could be due to acoustic phonons [8]. Under light excitation, there is no variation on the carriers' mobility between 200 and 300 K. On the other hand, for $T < 200$ K, the mobility clearly decreases under illumination. This decreasing observed on carrier mobility gives the main contribution to the negative photoconductivity, especially in the temperature region between 150 and 170 K. Below 150 K, the mobility under illumination is nearly constant, and the carrier concentration increasing should be more effective to the transport in this temperature region. The mobility decreasing is possible in degenerate systems due to carrier scattering at ionized states in the trap level [5]. Also, the effect of carrier-carrier scattering in the conduction band due to the enhancement of the carrier concentration (by a factor of ~10000) is possible [22].

Figure 3(b) presents the hole concentration under illumination and dark conditions. Without illumination, carrier concentration decreases as temperature decreases presenting the expected behavior for a semiconductor. Under illumination, the carrier concentration follows the same behavior as that observed in dark conditions when the temperature decreases from 300 K down to 200 K. Below 200 K, the carrier concentration is nearly constant but starts to increase below 100 K. This increasing is in the same temperature region where the huge effect of positive photoconductivity is observed and where the carrier mobility is nearly constant. This increasing in the carrier concentration is due to the increasing in the generation rate in this temperature region as will be seen later.

The normalized electrical resistance is presented in Fig. 3(c) where it is possible to observe a transition from an insulator to a metallic behavior when the sample is under illumination. This transition can be a result of the competition between the variations observed for the hole and carriers' mobility

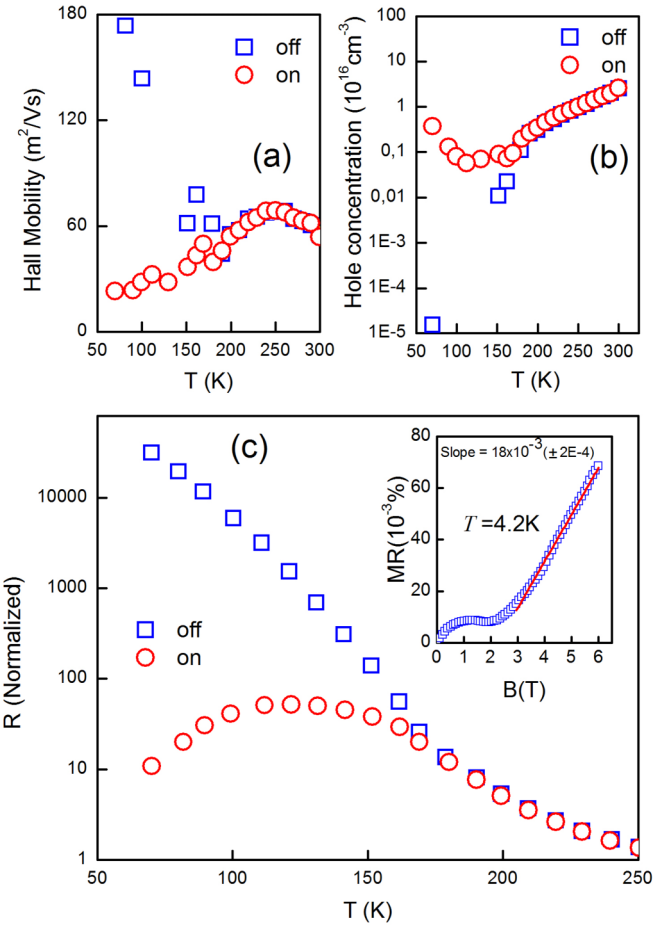

FIG. 3. (a) Hall mobility under illumination (on) and dark conditions (off). (b) Carrier concentration under illumination and dark conditions. The profiles observed in both figures reveal the effect of light at low temperatures (see the text for further explanations). (c) Normalized electrical resistance. It is possible to observe a transition from an insulator to a metallic behavior when the sample is under illumination during the cooling process.

presented in Figs. 3(a) and 3(b). It is important to point out that values of photoconductivity for temperatures of 170 and 150 K are much larger in Fig. 2(a) than in Fig. 3(c). In addition, for these temperatures, the photoconductivity is negative in Fig. 2(a), and this is absent in Fig. 3(c). As discussed earlier, there is a strong persistent photoconductivity effect that acts like a "memory effect" for temperatures below 130 K, i.e., the system does not recover its original state after the light is removed (see the arrows). To avoid the influence of this memory, we performed the photoconductivity measurements on different days for each temperature presented in Fig. 2(a). So, before each measurement, the system was cooling down from room temperature until the desired temperature. For Hall measurements present in Fig. 3, each point was measured on the same day with the light turned on during the whole time, starting from 77 K up to 300 K (open circles). The effect of memory, in this case, is present at low temperatures and can persist up to temperatures higher than 130 K. This memory effect contributes with a positive component to the conductivity (reduction of electrical resistance), and hence,

the total effect of the memory is to pull down the resistance curve presented in Fig. 3(c). In this situation, this effect can suppress the NPC effect observed in Fig. 2(a) for 150 and 170 K. In addition, it is possible that oxidation processes had played an important influence in the Hall measurements. The time interval between the photoconductivity and the Hall measurements was about 2 months. Oxidation processes in this time interval can reduce sample resistivity in several orders of magnitude depending on the temperature region [23]. For the sample with $x \sim 0.06$, the average electrical resistance was $\sim$230 kΩ during photoconductivity measurements and $\sim$130 kΩ during Hall measurements at 77 K. This resistance decreasing could also contribute to suppression of resistance increasing due to light.

The total variation of electrical conductivity is the contribution of the individual variations in valence and conduction bands due to the generation of electron-hole pairs under illumination,

$$\Delta\sigma = e(\mu_n \Delta n + \mu_p \Delta p), \tag{1}$$

where μ_n and μ_p are the electrons' and holes' mobility and Δn and Δp are the density of excess of electrons and holes, respectively. In the presence of trap centers, Δp becomes

$$\Delta p = \Delta n + \Delta n_d, \tag{2}$$

where Δn_d is the density of electrons trapped at the defect sites.

The generation and recombination rates from a level $i(= d$ or $4f$ for defect or $4f$ level) to the valence/conduction bands can be derived according to the expressions given in Ref. [15] such that the equations for the ratios between the generation and the recombination rates considering the $4f$ level are

$$g_{v4f}/r_{4fv} = \frac{(N_{4f} - n_{4f})N_v \exp\left(-\frac{E_g - \varepsilon_{4f}}{k_B T}\right)}{p n_{4f}}, \tag{3}$$

$$g_{4fc}/r_{c4f} = \frac{n_{4f} N_c \exp\left(-\frac{\varepsilon_{4f}}{k_B T}\right)}{n(N_{4f} - n_{4f})}, \tag{4}$$

and the equations for the ratios between the generation and the recombination rates considering the defect level are

$$g_{dc}/r_{cd} = \frac{n_d N_c \exp\left(-\frac{\varepsilon_d}{k_B T}\right)}{n(N_d - n_d)}, \tag{5}$$

$$g_{vd}/r_{dv} = \frac{(N_d - n_d)N_v \exp\left(-\frac{E_g - \varepsilon_d}{k_B T}\right)}{p n_d}, \tag{6}$$

where N_i is the density of the defect centers, n_i is the density of states occupied by electrons, and N_c and N_v are the effective density of states in the conduction and valence bands, respectively. The number of defects N_i can be estimated from magnetoresistance (MR) measurements. It is well known that for disordered systems MR can present a linear behavior instead of parabolic one [24]. The theoretical prediction is that the MR will behave linearly in magnetic-field B according to the expression $[\rho(B,T) - \rho(0,T)]/\rho(0,T) = N_i B/\pi n^2 e \rho(0,T)$. Hence, from the slope of the MR curve, one can extract the value of N_i.The inset in Fig. 3(c) shows the MR curve for a p-type $Pb_{1-x}Eu_xTe$ sample with $x = 0.06$ at 4.2 K. The MR clearly presents linear behavior for $B > 3$T. From the slope obtained from a linear fitting (solid line) we obtained $N_i \sim 5 \times 10^{17}\,\mathrm{cm}^{-3}$ where we used the values of $\rho(0{,}4.2\,\mathrm{K}) = 59\,\Omega\,\mathrm{cm}$ and $n \sim 10^{16}\,\mathrm{cm}^{-3}$.

It is not possible to know precisely the contribution from the $4f$ level and defect level to the total value of $N_i \sim 5 \times 10^{17}\,\mathrm{cm}^{-3}$. We made an approximation considering $N_{4f} = N_d = N_i/2$. If, for instance, we consider the contribution of 75% from the defect level and 25% from the $4f$ level, the final result does not change considerably. In fact, the amplitude of the ratios changes less than 1%.

In order to estimate the number of occupied states (n_d and n_{4f}) we used the Fermi-Dirac distribution $f_i(x,T) = 1/\{e^{[\varepsilon_i - \varepsilon_F(x)]/k_B T} + 1\}$, where ε_i assumes the values of 19.2 and 461.8 meV for the defect level and $4f$ level, respectively. The position of the $4f$ level can be calculated using the relation $\varepsilon_{4f}(x) = (0.34 + 2.03x)$, which is valid under the interval $0.06 < x \leqslant 0.60$ [19]. For the Fermi energy, we used the parabolic approximation $\varepsilon_F(x) = \hbar^2 k_F^2/2m_D$. For the effective mass m_D one has to take into account the anisotropy of the masses such that $m_D(x) = 4^{2/3}[m_l(x)m_t(x)^2]^{1/3}$, where $m_l(x) = (0.213 + 3.23x)m_e$ is the longitudinal mass and $m_t(x) = (0.0207 + 0.453x)m_e$ is the transversal mass with m_e being the electron mass [25]. We obtain $m_D(0.06) = 0.246m_e$. We calculate the Fermi wave number from the relation $k_F = (3\pi^4 n/4)^{1/3}$ [18]. We took an average of the distribution values between 300 and 77 K such that we have $[f_d(0.06{,}300) + f_d(0.06{,}77)]/2 = 0.15$. Hence, we used $n_d \sim 0.15N_i/2$. For the $4f$ level we have $[f_{4f}(0.06{,}300) + f_{4f}(0.06{,}77)]/2 = 0.30$. Hence, we considered $n_{4f} = 0.30N_i/2$. The energy gap as a function of temperature was calculated using the expression $E_g(x,T) = (189{,}7 + 0{,}48T^2\frac{(1-7{,}56x)}{T+29} + 4480x)$ [17].

The relation g_{v4f}/r_{4fv} is presented in Fig. 4(a) calculated using Eq. (3) in the range of 77–300 K. The curve increases as temperature decreases from 300 K down to 250 K, indicating a high generation from the valence band to the $4f$ level. This leads to an increase in conductivity in the valence band due to the excess of holes. As T decreases below 250 K, one observed a decreasing in the ratio indicating that the recombination process becomes more effective, giving a contribution to the NPC effect. In this same figure, we plot the relation g_{dc}/r_{cd} using Eq. (5). For high temperatures, the recombination from conduction band to the defect level is much higher than the generation from the defect level to the conduction band. This indicates that this process gives no positive contribution to conductivity. However, as temperature decreases below $\sim$230 K, there is a significant increase in the relation g_{dc}/r_{cd}, which gives a positive contribution to the conductivity. Figure 4(b) shows the calculated values for the relation g_{4fc}/r_{c4f} using Eq. (4). From this figure, one observes that the recombination from conduction band to $4f$ level is more effective than the generation from the $4f$ level to the conduction band in the whole range of temperatures investigated. This indicates that this mechanism gives a negative contribution to the conductivity and can be one source of the NPC effect. Figure 4(c) presents the ratio g_{vd}/r_{dv} calculated using Eq. (6) and shows that the

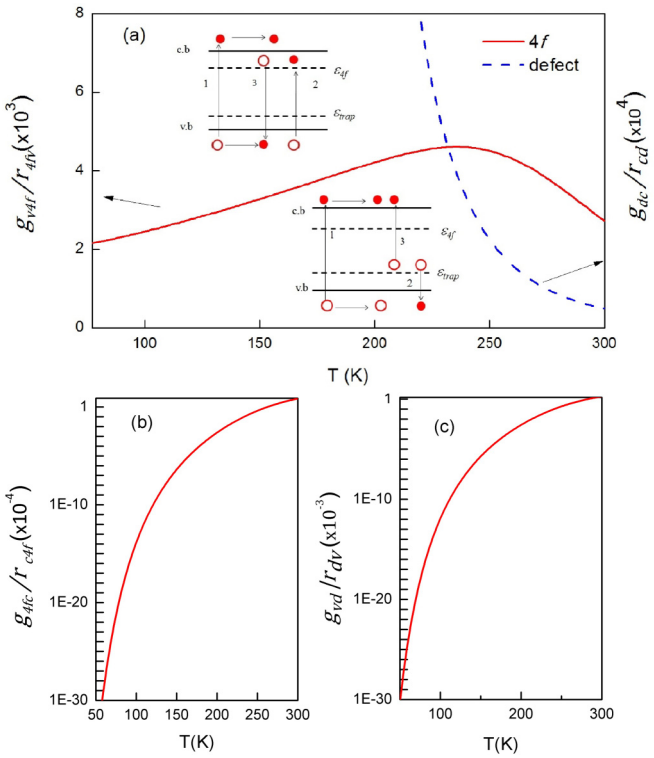

FIG. 4. (a) The ratio g_{v4f}/r_{4fv} calculated using Eq. (3), and the ratio g_{dc}/r_{cd} calculated using Eq. (5) in the range of 77–300 K. (b) Calculated values for the ratio g_{4fc}/r_{c4f} using Eq. (4). (c) Calculated values for g_{vd}/r_{dv} using Eq. (6). The insets present a pictorial representation of the generation and recombination processes (see the text for further explanation).

recombination from the defect level to the valence band is more effective than the generation from the valence band to the trap level. This process also gives a contribution to the negative photoconductivity. Clearly, there is a competition between the processes which results in the different profiles of photoconductivity observed in Fig. 2(a). In order to show a pictorial description of the processes describe above, we present in the insets of Fig. 4(a) a simplified diagram of the generation and recombination rates. The upper inset shows the generated electrons from valence band to conduction band under light excitation indicated by process 1. This process naturally gives rise to a positive photoconductivity, commonly observed in semiconductors. Electrons also are excited to the $4f$ level, leaving additional holes in the valence bands (process 2). After some time, electrons recombine back from the $4f$ level to the valence band (process 3). Processes 1 and 2 contribute to a positive photoconductivity, whereas process 3 contributes to the NPC effect. This process 3 is relevant only for temperatures below ∼230 K as observed in Fig. 4(a). In the lower inset, process 1 is similar to process 1 in the last case. The recombination from the defect level is indicated in process 2, which seems to dominate over the generation according to Fig. 4(c). For this process, when light is switched off, the recombination diminishes, which also contributes to the peaks observed in the curves indicated by the arrows in Fig. 2(a). This transient process vanishes in a very short period of time. Process 3 indicates the generation from the defect level to the conduction band. According to calculated values (solid curve), process 3 becomes more relevant as temperature decreases. To summarize, the positive contribution dominates for temperatures higher than 200 K due to the excess of holes generated in the valence band (high value of g_{v4f}/r_{4fv}). Below ∼230 K down to 150 K, approximately, the negative photoconductivity dominates due to the low relation $g_{v4f} < r_{4fv}$ and due to the reduction of carrier mobility as discussed earlier. In the temperature region of 77–150 K, approximately, the positive photoconductivity takes place again with an amplitude hundreds of times higher than those observed close to room temperature, mainly caused due to the excess of electrons in the conduction band (high values of g_{dc}/r_{cd}).

IV. CONCLUSIONS

We observed a clear transition from negative to positive photoconductivity for p-type $Pb_{1-x}Eu_xTe$ films for $x = 0.01$, 0.02, 0.03, 0.05, and 0.06 at $T = 300$ K under illumination of infrared light. This transition is related to the metal-insulator transition that occurs due to the disorder originated from the introduction of Eu atoms. According to the analysis performed for the p-type $Pb_{1-x}Eu_xTe$ film with $x = 0.06$, we concluded that the PPC and NPC effects at different temperatures are a consequence of the reduction or increase in electrons and holes in conduction and valence bands, respectively, due the influence of the two trap levels (the $4f$ and defect levels) in the dynamics of recombination rates, which also are deeply temperature dependent. The p-type $Pb_{1-x}Eu_xTe$ film with $x = 0.06$ by results of photoconductivity revealed to be a material with interesting physical properties and a promising candidate for applications in the development of new sensors and photodetectors.

ACKNOWLEDGMENTS

We would like to thank CAPES, CNPq, and FAPEMIG (Grant No. APQ-00623-14) for financial support.

[1] M. M. Furchi, D. K. Polyushkin, A. Pospischil, and T. Mueller, Mechanisms of photoconductivity in atomically thin MoS_2, Nano Lett. **14**, 6165 (2014).

[2] R. L. Field, III, Y. Jin, H. Cheng, T. Dannecker, R. M. Jock, Y. Q. Wang, C. Kurdak, and R. S. Goldman, Influence of N incorporation on persistent photoconductivity in GaAsN alloys, Phys. Rev B **87**, 155303 (2013).

[3] Y. Yang, X. Peng, H. S. Kim, T. Kim, S. Jeon, H. K. Kang, W. Choi, J. Song, Y. J. Doh, and D. Yu, Hot carried trapping induced negative phtoconductance in InAs Nanowires toward novel nonvolatile memory, Nano Lett. **15**, 5875 (2015).

[4] R. Jaramillo, M.-J. Sher, B. K. Ofori-Okai, V. Steinmann, C. Yang, K. Hartman, K. A. Nelson, A. M. Lindenberg, R. G. Gordon, and T. Buonassisi, Transient terahertz

photoconductivity measurements of minority-carrier lifetime in tin sulfide thin films: Advanced metrology for an early stage photovoltaic material, J. Appl. Phys. **119**, 035101 (2016).

[5] P. C. Wei, S. Chattopadhyay, M. D. Yang, S. C. Tong, J. L. Shen, C.Y. Lu, H. C. Shih, L. C. Chen, and K. H. Chen, Room temperature negative photoconductivity in degenerate InN thin films with a supergap excitation, Phys. Rev. B **81**, 045306 (2010).

[6] C. H. Lui, A. J. Frenzel, D. V. Pilon, Y.-H. Lee, X. Ling, G. M. Akselrod, J. Kong, and N. Gedik, Trion- Induced Negative Photoconductivity in Nonolayer MoS_2, Phys. Rev. Lett. **113**, 166801 (2014).

[7] R. Sreekumar, R. Jayakrishnan, C. S. Kartha, and K. P. Vijayakumar, Anomalous photoconductivity in gamma In_2Se_3, J. Appl. Phys. **100**, 033707 (2006).

[8] N. Gogurla, A. K. Sinha, D. Naskar, S. C. Kundub, and S. K. Ray, Metal nanoparticles triggered persistent negative photoconductivity in silk protein hydrogels, Nanoscale **8**, 7695 (2016).

[9] H. Nakanishi, K. J. M. Bishop, B. Kowalczyk, A. Nitzan, E. A. Weiss, K. V. Tretiakov, M. M. Apodaca, R. Klajn, F. Stoddart, and B. A. Grzybowski, Photoconductance and inverse photoconductance in films of functionalized metal nanoparticles, Nature (London) **460**, 371 (2009).

[10] M. Nowak, K. Mistewicz, A. Nowrot, P. Szperlich, M. Jesionek, and A. Starczewska, Transient characteristics and negative photoconductivity of SbSI humidity sensor, Sens. Actuators A: Phys. **210**, 32 (2014).

[11] L. Guo, X. Wang, L. Feng, X. Zheng, G. Chen, X. Yang, F. Xu, N. Tang, L. Lu, W. Ge, and B. Shen, Temperature sensitive photoconductivity observed in InN layers, Appl. Phys. Lett. **102**, 072103 (2013).

[12] B. A. Akimov, V. A. Bogoyavlenskii, V. A. Vasil'kov, L. I. Ryabova, and D. R. Khokhlov, Recombination at mixed-valence impurity centers in PbTe(Ga) epitaxial layers, Phys. Solid State **47**, 166 (2005).

[13] B. A. Akimov and V. A. Bogoyavlenskiy, Experimental study of negative photoconductivity in n-PbTe(Ga) epitaxial films, Phys. Rev. B **61**, 16045 (2000).

[14] E. P. Skipetrov, E. Zvereva, L. Skipetrova, and E. Slyn'ko, Impurity-induced photoconductivity in gallium-doped $Pb_{1-x}Ge_xTe$ alloys, Physica B: Condens. Matter **302**, 393 (2001).

[15] K. Lischka, R. Durstberger, G. Lindemann, and H. Staudinger, Defect states in $Pb_{1-x}Sn_xTe$, Phys. Status Solidi B **123**, 319 (1984).

[16] M. A. B. Tavares, M. J. da Silva, M. L. Peres, S. de Castro, D. A. W. Soares, A. K. Okazaki, C. I. Fornari, P. H. O. Rappl, and E. Abramof, Investigation of negative photoconductivity in p-type $Pb_{1-x}Sn_xTe$ film, Appl. Phys. Lett. **110**, 042102 (2017).

[17] S. Yuan, H. Krenn, G. Springholz, Y. Ueta, G. Bauer, and P. J. McCann, Magnetoreflectivity of $Pb_{1-x}Eu_xTe$ epilayers and $PbTe/Pb_{1-x}Eu_xTe$ multiple quantum wells, Phys. Rev. B **55**, 4607 (1997).

[18] J. A. H. Coaquira, V. A. Chitta, N. F. Oliveira, Jr., P. H. O. Rappl, A. Y. Ueta, E. Abramof, and G. Bauer, Electrical characterization of p-type $Pb_{1-x}Eu_xTe$, J. Supercond. **16**, 115 (2003).

[19] H. Krenn, W. Herbst, H. Pascher, Y. Ueta, G. Springholz, and G. Bauer, Interband Faraday and Kerr rotation and magnetization of $Pb_{1-x}Eu_xTe$ in the concentration range $0 \leqslant x \leqslant 1$, Phys. Rev. B **60**, 8117 (1999).

[20] M. L. Peres, R. M. Rubinger, L. H. Ribeiro, C. P. L. Rubinger, G. M. Ribeiro, V. A. Chitta, P. H. O. Rappl, and E Abramof, Conduction mechanisms in p-type $Pb_{1-x}Eu_xTe$ alloys in the insulator regime, J. Appl. Phys. **111**, 123708 (2012).

[21] M. L. Peres, V. A. Chitta, N. F. Oliveira, Jr., D. K. Maude, P. H. O. Rappl, A. Y. Ueta, and E. Abramof, Antilocalization of hole carriers in $Pb_{1-x}Eu_xTe$ alloys in the metallic regime, Phys. Rev. B **79**, 085309 (2009).

[22] D. M. Zayachuk, The dominant mechanisms of charge-carrier scattering in lead telluride, Semiconductors **31**, 173 (1997).

[23] J. Wang, J. Hu, P. Becla, A. M. Agarwal, and L. C. Kimerling, Room-temperature oxygen sensitization in highly textured, nanocrystalline PbTe films: A mechanistic study, J. Appl. Phys. **110**, 083719 (2011).

[24] A. A. Abrikosov, Quantum magnetoresistance, Phys. Rev. B **58**, 2788 (1998).

[25] A. Prinz, G. Brunthaler, Y. Ueta, G. Springholz, G. Bauer, G. Grabecki, and T. Dietl, Electron localization in n-$Pb_{1-x}Eu_xTe$, Phys. Rev. B **59**, 12983 (1999).